Atomic scale analysis of N dopants in InAs

T. J. F. Verstijnen,[1,*] D. Tjeertes,[1] E.G. Banfi,[1] Q. Zhuang,[2] and P. M. Koenraad[1]

[1]*Department of Applied Physics and Science Education, Eindhoven University of Technology, P.O. Box 513, 5600 MB Eindhoven, The Netherlands*

[2]*Physics Department, Lancaster University, Lancaster LA1 4YB, United Kingdom*

(Dated: June 5, 2023)

The band gap of most III-V semiconductors is strongly reduced with the introduction of only a few percent of N, even if the III-N alloy has a much bigger band gap. N impurities in InAs introduce an impurity state around 1 eV above the conduction band minimum, much deeper in the band than in other III-V materials. Topographic scanning tunneling spectroscopy measurements (STS) and areal spectroscopy measurements performed on N atoms up to two layers below the (110) surface of InAs show a reduction of the resonance energy of the N atom with increasing depth. This is attributed to tip induced band bending, pulling the N states up at positive bias and acting most strongly on surface N atoms. STS measurements obtained on undoped InAs and N-doped InAs show a band gap reduction of <0.1 eV. Spacial imaging of features corresponding to N dopants up to two layers below the surface are also compared to density functional theory simulations and show excellent correspondence. Spectroscopy maps of N atoms up to two layers below the surface provide a high resolution spatial and spectroscopic view of the N atoms. Here the characteristic shape of the N atoms in different layers below the surface is observed as an enhancement of the dI/dV signal compared to the InAs background. At energies above the enhancement a reduction of the dI/dV is observed, which has the same shape and size as the enhancement. This shows that the redistribution of density of states caused by the N impurities is mainly energetic in nature.

I. INTRODUCTION

The band gap of most III-V semiconductors is strongly reduced with the introduction of only a few percent of N, even if the III-N alloy has a much bigger band gap[1–3]. Multiple models are used to describe this reduction of the band gap. One of the most popular is the band anti-crossing model[4], which models an interaction between the lowest energy conduction band states and the states introduced by the N atoms. Another model considers a linear combination of isolated nitrogen states (LCINS) and the conduction band minimum (CBM)[5,6].

On the atomic scale the N affects the local structural and electronic properties of the host material. N atoms on group V sites are iso-electronic dopants, they do not introduce new charge carriers to the material. Instead their influence on the material properties comes from the difference in atomic size and electro-negativity compared to the group V atom they replace. N is the smallest group V atom, so when it replaces another group V atom it will induce local strain in the lattice. Due to this large lattice mismatch, alloys like this are called highly mismatched alloys (HMA's). The N atom is also much more electro-negative than the other group V atoms, and as such will influence the electronic states around it.

Depending on the band gap of the host material the N state is introduced at a different energy position compared to the CBM. In GaP the N states are introduced below the CBM, in the band gap[7]. For GaAs the N states are located around the CBM, with isolated N atoms introducing a state 0.23 eV above the CBM, while N pairs can introduce states in the band gap[8,9]. For InAs the situation is different than GaP and GaAs, due to the small band gap (0.354 eV), the N states are introduced around 1 eV above the conduction band edge[10,11].

The behavior of N in GaAs, where the Ga atoms surrounding the N atoms are pulled towards it, has been studied in detail. This effect can be clearly seen in cross-sectional scanning tunneling microscopy (X-STM) measurements of the (110) surface of N doped GaAs[12–14], which has been confirmed by density function theory (DFT) calculations[15]. With X-STM also the local density of states (LDOS) around the N atoms can be observed, which has been described in detail for N in GaAs[16,17].

The band gap reduction of InAsN has been well described by the BAC model[18], but the behavior at the atomic scale remains to be studied. It is also interesting to know how iso-electronic impurities behave deep in the band and to see if this behavior differs from more shallow iso-electronic dopants. The lattice constant of InAs is 6.06 Å, which is about 7% larger than GaAs. Since the effects that the N atoms have on the host material is partially based on the locally induced strain, it is expected that the effects will be of different strength in InAs compared to GaAs. In atoms are also less electronegative than Ga atoms, 1.78 versus 1.81, respectively. These are both considerably different than the 3.04 of N. This could cause differences in the N states when comparing GaAs and InAs[19].

In this paper we study N atoms in InAs at the atomic scale with X-STM. We study the band gap characteristics observed when going from a region of undoped InAs to N-doped InAs. We observe the LDOS around N atoms in different layers below the (110) surface and compare this with previous results obtained for N in GaAs. The energetic position of the states corresponding to N atoms at different depths with respect to the surface are also studied and compared to Density Functional Theory (DFT) simulations. Lastly we provide scanning tunneling spectroscopy (STS) curves and current imaging tunneling spectroscopy (CITS) maps of N atoms in different layers below the surface. This provides a deeper understanding of the differences between N in GaAs and InAs at the atomic scale.

II. METHODS

A. Experimental Methods

For this study 200 nm thick bulk doped $InAs_{1-x}N_x$ layers were grown on (100) n^+-doped InAs substrates by molecular beam epitaxy with a 200 nm undoped InAs buffer layer in between the substrate and the $InAs_{1-x}N_x$ layer. The nominal N concentration in the sample was 2.29%. X-STM measurements were performed with a commercial Omicron LT-STM, which has two bath cryostats. The outer cryostat is filled with liquid nitrogen (LN_2) and has a hold time of approximately 12 hours. The inner cryostat can be filled with either liquid LN_2 or liquid helium (LHe) to cool down to 77K or 5K, respectively. This cryostat has a hold time of about 24 hours when filled with LHe. The hold time of the outer cryostat is a limiting factor for the length spectroscopy measurements. Most topographic measurements were performed at 77K, while the high-resolution spectroscopic measurements were performed at 5K to provide the highest stability.

Samples were brought into the ultra-high vacuum ($<1\times10^{-10}$ mbar) of the STM chamber before cleaving them and revealing a clean (110) cross-section of the sample. STM tips were prepared by electro-chemical etching of polycrystalline tungsten wire. After loading into the STM system they are annealed and sputtered with argon ions to remove oxide layers and improve tip quality.

STS curves are obtained by first stabilizing the tip at a specific bias voltage and tunnel current and then turning the feedback loop off and sweeping the voltage over a selected range. dI/dV are obtained through a lock-in amplifier (Stanford Research Systems SR510), by applying a 1027 Hz modulation signal with an amplitude of 10 mV to the sample bias. The relation between the dI/dV signal and the LDOS can be described with the following formula,

$$\frac{dI}{dV}(eV) \propto \rho_s(E_{F,s}+eV)\; exp(-2\kappa z_{tip}) \qquad (1)$$

where V is the applied bias voltage, ρ_s is the LDOS of the sample, $E_{F,s}$ the Fermi energy of the sample, κ the inverse decay length in vacuum and z_{tip} the tip-sample distance. Since the tip-sample distance is kept constant during an STS curve, the dI/dV signal is directly proportional to the LDOS of the sample. When comparing STS curves it is important to consider that z_{tip} can be slightly different, affecting the dI/dV signal by the way of topography cross-talk. The stabilization voltage is chosen in such a way that the cross-talk is minimal and effects of cross-talk are taken into consideration when discussing our STS results.

B. Computational Methods

The DFT simulations are carried out in the framework of the Vienna Ab Initio Simulation Package (VASP)[20]. In order to describe the exchange correlation interaction between electrons the Generalized Gradient Approximation (GGA) is used, specifically a Perdew-Burke-Ernzerhof (PBE) functional[21]. The Ion-electron interaction is described using the Projector-Augmented-Wave (PAW) method[22]. These functionals lead to an InAs lattice constant of 6.22 Å. This is an overestimation of the experimental lattice constant which is expected for PAW-PBE functionals[23]. We now generate supercells to describe N dopants at different depths below the (110) surface of InAs. These cells are generated from a 4×4 InAs (110) surface supercell that is 7 atomic layers thick. In this cell consisting of 224 atoms, 12 Å of vacuum is introduced to properly simulate the surface behavior. This pure InAs surface cell will from here on be referred to as the reference cell. A N dopant is now introduced at three different group V lattice sites in the reference cell: in the surface layer, N0, one layer below the surface, N1, and two layers below the surface layer, N2. The reference cell and the N doped cells are now left to relax until the force on each atom is less than 0.05 eV/Å. This is done using a Monkhorst-Pack grid of $3\times3\times1$[24] for the sampling of the Brillouin Zone. The cutoff energy used for the plane-wave-basis set is 400 eV. In order to improve the convergence of the simulations a Gaussian smearing of 0.03 eV in the occupation of the orbitals is also implemented. For the reference cell we find a band gap of 0.382 eV while for the N doped cells we find a band gap of 0.371 eV. It is not uncommon for GGA-PBE DFT calculations of InAs made in VASP to find a finite band gap[25]. The Local Density Of States (LDOS) is calculated on the atoms in the different doped supercells and compared to the As atom at the same lattice site in the reference cell. This way we can investigate the energy profile of the states corresponding to the N dopant at different depths.

III. RESULTS AND DISCUSSION

A. {110} Surfaces

The {110} surfaces of zinc-blende semiconductors consist of zigzag rows of alternating group III and V atoms. In the case of this paper these are In and As atoms, respectively. These rows are oriented perpendicular to the [001] direction. Depending on whether the (110) or $(1\bar{1}0)$, the zigzag rows first show the In atoms and then the As atoms when following the [001] axis, or vice versa. From the side view, multiple layers can be defined with respect to the surface. We define the surface layer as layer 0, and all other planes are defined by their depth below the surface plane.

B. Long range spectroscopy

To observe the band gap reducing effects of N we have taken STS spectra on both the undoped InAs buffer layer and the N-doped InAs layer, which can be seen in Fig. 1(a) as the orange and blue curves, respectively. These curves are averages over 9 dI/dV curves in the respective sample area. The curves were obtained by stabilizing the tip at a bias voltage of -2.0 V and a tunnel current of 50 pA. Spectroscopic I(V)

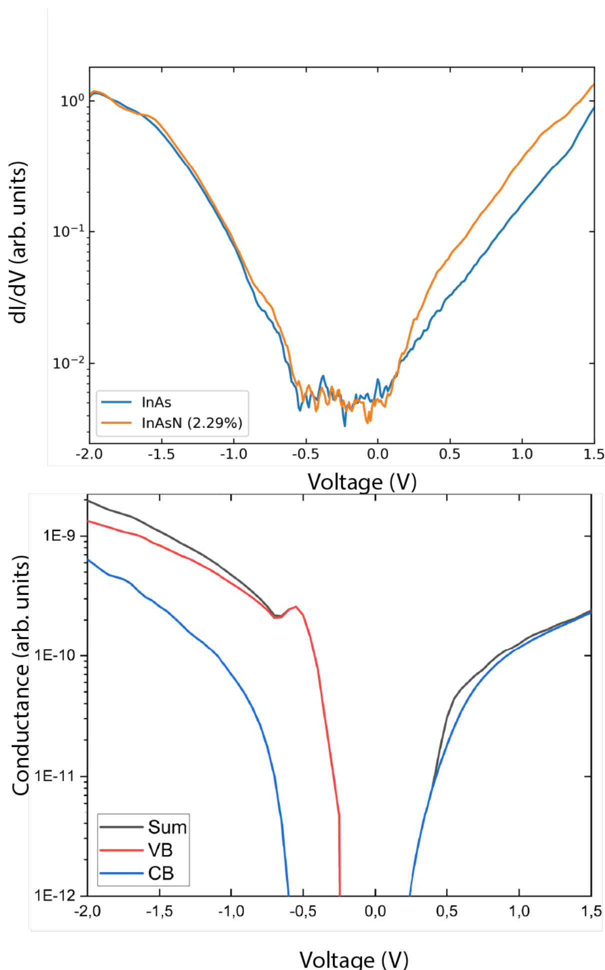

FIG. 1. In (a) the logarithmic plot of STS curves taken on undoped InAs and N-doped InAs is shown. Both curves were obtained by averaging 9 dI/dV curves in the respective sample area. In (b), the simulated conductance of the (110) InAs surface is presented. The conductance from the Conduction and Valence bands, CB and VB respectively, are shown as well as as the total conductance, Sum. These simulations were performed with the SEMITIP code developed by Feenstra et al.[26–28]. The following simulation parameters were used: a tip sample distance of 0.5nm, a temperature of 4K and a doping concentration of 2E18, as reported by the growers.

curves were then obtained at a series of bias voltages ranging from -2.0 V to $+1.5$ V. At negative voltages the curves overlap from -2.0 to -0.8 V, from where the dI/dV signal on the N-doped layer is slightly higher. The dI/dV signal is stronger for the N-doped InAs at all positive voltages. It is well known that the cleaved surfaces of InAs often exhibit an intrinsic electron accumulation layer[29–31]. The reason for this electron accumulation layer is still a topic of discussion however, one possible reason given is defects in the (110) surface of InAs[32]. In our measurements we observe a nearly defect free surface of InAs and N doped InAs, this will affect the amount of accumulation. When an STM tip is introduced near a surface, it strongly affects the bands present at this surface, even at zero tip bias. This means that, dependent on the work function of the tip, the electron accumulation layer at the surface of InAs is influenced by the presence of the STM tip[33]. Therefore we cannot say for certain how large or small the effect of electron accumulation is at the surface we measure in these STS curves. Because of these factors that can influence the STS measurements, it is important to understand what parts of the dI/dV spectrum originate from what part of the band structure of the material. This is why we performed simulations using the code developed by Feenstra et al.[26–28]. The results of these simulations are shown in Fig. 1(b). These simulations show that the conductance when tunneling with a positive bias mainly originates from conduction band states, with only a small contribution from the VB at -0.7 V. For negative biases, two clear regimes of tunneling can be identified. First, starting at -0.25V, the valence band states dominate the conductance alone. At -0.6V however, a contribution from conduction band states starts to appear as well as an abrupt change in VB conductance. This corresponds nicely with the experimentally obtained dI/dV curves since there is a clear change in slope around -0.7 V for both the N doped and clean InAs STS curves leading to a shoulder in these curves around -0.7 V. This change in slope, we can understand from the simulations, is caused in part by the additional tunneling available from conduction band states at this bias. We now compare the spectra obtained on clean InAs and N-doped InAs at different biases. At positive bias, where electrons tunnel from the filled states in the tip to empty conduction band states of the sample, a large difference in the strength of the dI/dV signal is observed. This is present for all positive voltages where the dI/dV signal is higher than the signal from the accumulation layer. This difference can be understood by considering the effect of N doping on band structure of InAs. The BAC model describes the introduction of the N state and the resulting splitting and energy lowering of the conduction band. This downward shift in energy and the introduction of the N state strongly contribute to the enhanced DOS to tunnel into at all CB energies when comparing intrinsic InAs and N-doped InAs, which is what we observe in Fig. 1(a). For negative bias, a small shift at the shoulder described earlier is observed. The STS curve of the N doped region is shifted to more positive voltages compared to the clean InAs STS curve by less than 0.1 eV. The horizontal shift of the N doped InAs STS curve at -0.7V leads to a small reduction in the apparent band gap. At 2.29% N, a band gap reduction of 0.08 V is expected[18]. Additional absorption and PL characterization of the sample by the growers also showed band gap reductions of 0.05-0.10 eV[34].The fact that we see a part of the band gap reduction at negative voltages can be understood in the following way: If the Fermi energy remains locked to the conduction band minimum (as is to be expected in n-type material) we expect that tunneling from the valence band to the STM tip will occur at a smaller (negative) voltage. In reality we expect that this is probably not 100% correct but at least a part of the band gap reduction is expected to show up as a shift of the valence band tunneling. For positive bias, the tunneling is expected to start at 0.0V due to the fact that the material is n-type. However, the STM has a limited noise floor. Therefore, we do not see the proper zero dI/dV point here as we are limited in our current

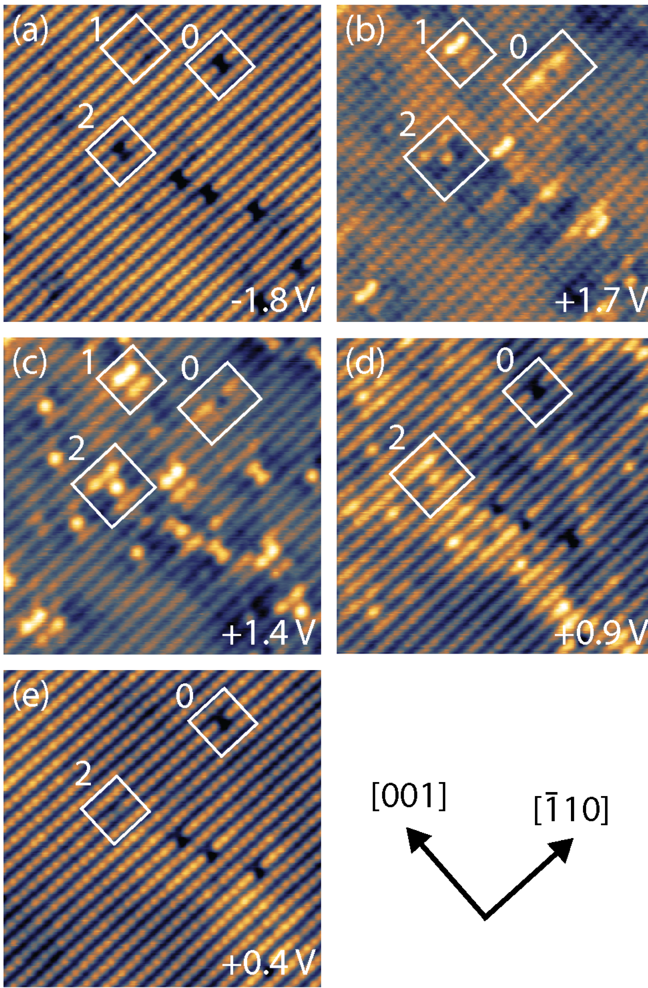

FIG. 2. 21 nm by 21 nm STM images of sample A0201 (2.29%) obtained at different bias voltages. (a), (b), (c), (d) and (e) are obtained at −1.8 V, +1.8 V, +1.4 V, +0.9 V and +0.4 V, respectively. All images were obtained with a set point current of 50 pA at 77K. One example of an N atom in each layer is marked with the number indicating their respective layer.

resolution. This does mean that we do not expect to observe the band gap reduction on the positive bias side of our STS measurements, since for both materials tunneling is expected to start at 0.0V.

C. Voltage dependent topography

The N containing bulk layer is imaged at different bias voltages to find the resonance energies and voltage dependence. At negative bias electrons tunnel from filled states of the sample into the tip. Since the states introduced by the N are located far above the conduction band minimum, we see little effect of this at negative bias. Instead topographic effects dominate the observed contrast, which are well documented for N in III/V semiconductors, with N atoms causing depressions of the (110) surface[12–14].

At positive bias electrons tunnel from filled states in the tip to the empty states of the samples. These empty states in the sample will include the N-induced states, which causes an enhancement of the tunnel current at specific voltages around the N atoms. This has been well documented for N in GaAs[16,17]. Based on the observations at negative and positive voltage the N features are identified as residing in a specific layer with respect to the surface. In Fig. 2 a few N atoms are marked with the layer they reside in, with 0 indicating an N atom in the surface and 1 indicating an N atom one layer below the surface et cetera. The observed contrast at both positive and negative bias is remarkably similar to N in GaAs. These features are also compared to simulated STM images using DFT. These simulated STM images are shown in Fig. 3(b), (e) and (h) as well as the features marked with N0, N1 and N2 as shown in fig. 2 in Fig. 3(a), (d) and (g) . These simulated STM images are simulated at 3 Å above the slab surface which is comparable to typical tip-sample distances. They are simulated for a bias voltage of +0.5 eV. The resemblance between the simulated images shown here and the experimental features is remarkable. Both the shape and size of the features matches very well between the two. In the case of N0, the feature is extended only in the [1$\bar{1}$0] direction with a dark spot on the location of the N dopant. In the case of N1, both the simulated and experimental feature consist of two pairs of two lobed bright contrasts with the two lobes in the [001] direction being brighter. In the case of N2 we see in both cases that the feature is extended over 3 corrugation rows. There is a bright middle atom right above where the N atom is present with two side lobes in the [001] and [00$\bar{1}$] direction of which the side lobe in the [001] direction is the brightest. The difference in bias voltage at which the states show the highest change in LDOS between simulation and experiment can be understood thanks to the way the STM tip interacts with the sample states. During positive bias imaging, the STM tip bends the N related states up in energy. This means that in STM imaging the N related states could show a resonance at higher energies. The simulated features of N0, N1 and N2 for a bias voltage of +2.0V are also presented in Fig. 3(c), (f) and (i). Here we see that the LDOS is weaker in the area that was the brightest in Fig. 3(b), (e) and (h), especially in the case of N1 and N2. This means that a reduction in LDOS with the shape of the original feature could be observed in STM measurements for bias voltages above the resonance of the feature.

At high positive voltage (+1.7 V), as seen in Fig. 2(a), mainly the surface N atoms and N atoms one layer below the surface are observed. In Fig. 2(c) the observed contrast at a bias voltage of +1.4 V is displayed. Here deeper N atoms have a more pronounced contrast than in Fig. 2(b) and the bright contrast of the surface N atom has decreased. In Fig. 2(d) most of the strong localized contrast has disappeared, and instead a diffuse contrast is observed around various deep lying N atoms. In Fig. 2(e) the electronic contrast around the N atoms has completely disappeared. Since we can already tunnel into the CB at +0.4V like shown in Fig. 2(e) and the features corresponding to the N dopants show up at higher voltages, the N related states are present deep in the CB.

The size of the observed LDOS around the N atoms is

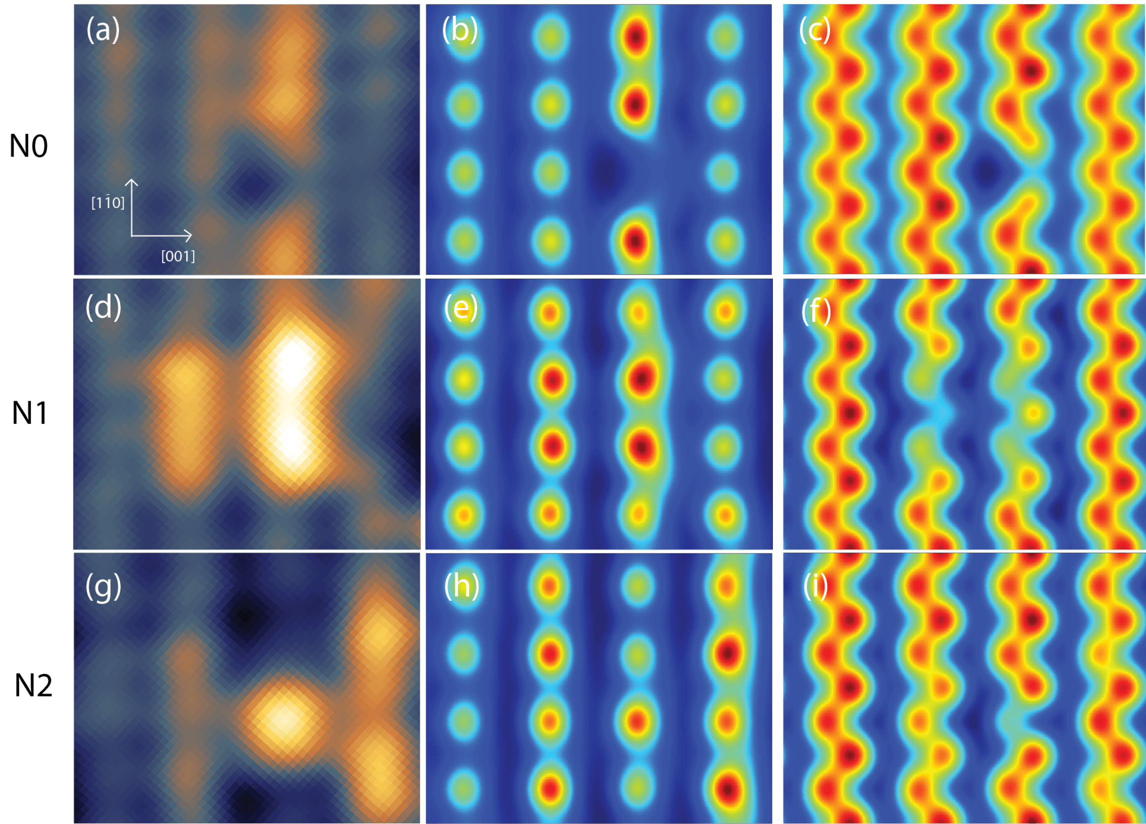

FIG. 3. 2.5 by 2.0 nm simulated STM images and experimental STM images of N dopants in the surface layer, (a), (b) and (c), one layer below the surface, (e) , (e) and (f) and two layers below the surface, (g), (h) and (i). The simulated images were generated at a height of 3 Å above the slab surface. The simulated STM images shown in (b), (e) and (h) are generated at a bias voltage of +0.5V. The simulated STM images shown in (c), (f) and (i) are generated at a bias voltage of +2.0V. The experimental STM images shown are obtained for a bias voltage of +1.5V and a temperature of 77K and a current of 50 pA..

nearly the same as for N atoms in GaAs. This can be explained by considering the zinc-blende crystal structure. Both InAs and GaAs have the zinc-blende structure in which the N atoms are embedded on a group V position. The LDOS around the N atoms propagates along the atomic bonds in this lattice. The deeper the N atom is located with respect to the surface, the more spatially extended the LDOS has become. Since this LDOS extension only happens along the atomic bonds, there will be no difference in the shape and size of the observed LDOS when comparing N atoms in InAs and GaAs. The main difference could be in the strength of the LDOS of the N state, which is not feasible to compare between InAs and GaAs.

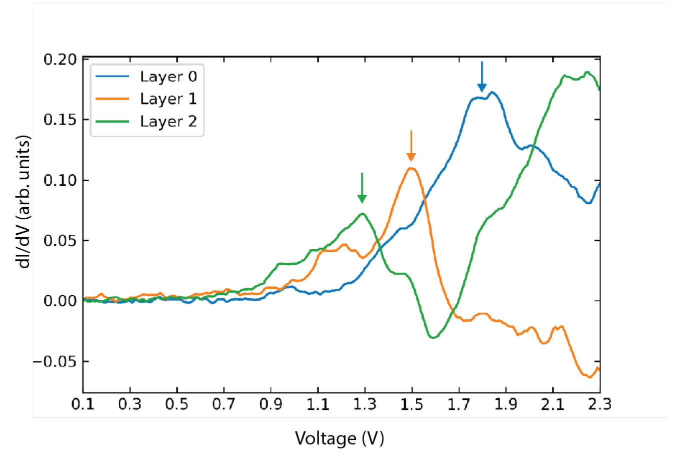

FIG. 4. STS spectra (dI/dV) taken at point of strongest contrast for N atoms in different layers with respect to the surface. Curves displayed are for N atoms in the surface layer (blue), one layer below (orange) and two layers below (green). The N resonance in each curve is marked with an arrow in the respective color of the curve. Spectra were taken with the same tip and have an InAs background spectrum subtracted. All curves are an average of five spectra.

D. Spectroscopy curves

STS spectra provide information on the relative position of energy states of N atoms. In Fig. 4 the STS spectra taken on the feature corresponding to an N atom in the surface (blue), one layer below the surface (orange) and two layers below the surface (green) are presented. STS curves were obtained with a stabilization voltage of +2.3 V and a set point current of 50 pA. The stabilization voltage of the STS curves is ideally set

so that little electronic contrast is visible. This electronic contrast would lead to topographic cross-talk in the dI/dV curves. Here however, at +2.3 V, some of the electronic contrast of the N atoms is still visible, especially for the N atom in the surface and one layer below the surface. At higher positive voltages the contrast of the N atoms became weaker, but tip stability decreased drastically resulting in unreliable results. Another option would be to stabilize the tip at a low positive bias, which also exhibits limited to no electronic contrast as shown in Fig. 2(e). The reason that was not done is that the tip will be very close to the surface, due to the limited conductivity at this bias, meaning that when the bias is increased during the STS measurement the current will quickly saturate the pre-amplifier which is limited to 3.3 nA. We consider the stabilizing voltage of +2.3 V as the best compromise. This does mean that some topographic cross-talk is influencing the dI/dV strength.

All the curves in Fig. 4 have been modified by subtracting an average of background curves taken on clean InAs. In this way the y-axis indicates whether the LDOS at the N atoms is higher (>0) or lower (<0) than the InAs background. The surface layer N shows a broad peak with a maximum at +1.8 V and shows a higher LDOS than the InAs background from +2.3 to +1.0 V. The N atom one layer below the surface shows a clear peak at +1.5 V, with a shoulder ranging to +1.0 V. At the higher voltage side the dI/dV signal is lower than the background. For N atoms two layers below the surface a peak in the dI/dV signal can be seen at a bias of +1.3 V with a broad shoulder ranging to +0.9 V. Around +1.6 V a dip in the dI/dV signal is observed, which goes below the InAs background, such dips have also been observed by Ivanova *et al.*[35] in both experimental and theoretical work. At higher positive voltage a peak in the dI/dV signal is observed.

From the dI/dV signal at the stabilizing voltage of +2.3 V it can already be seen that some topographic cross-talk is present, since ideally the curves would have the same dI/dV. Nonetheless, these curves show a clear trend of the peak energy decreasing as the N atom is located deeper below the (110) surface. The peaks go from +1.8 V for the surface N, to +1.5 V and +1.2 V for the N atoms one and two layers below the surface, respectively. The enhancement of the LDOS also continues to lower voltages as the N atom is located deeper below the surface. For the surface N atom the enhancement stops around +1.2 V, for the N atom one layer below the surface around +1.0 V and for the N two layers below the surface around +0.8 V. The peak position with respect to the CBM is not captured in these measurements. Considering that the N state in InAs is located about 1 eV above the CBM, even the peak of the N atom in layer 2 has a larger energy then this, indicating that TIBB still plays a role. It is expected that for N atoms in deeper layers the peak energy goes towards 1 eV above the CBM.

We now compare the experimental results to the DFT calculations that were performed as described in section II B. A schematic view of the surface of the various different N doped supercells is presented in Fig. 6 as well as a side view of the (110) surface that indicates where the N dopants are present in the different doped supercells.

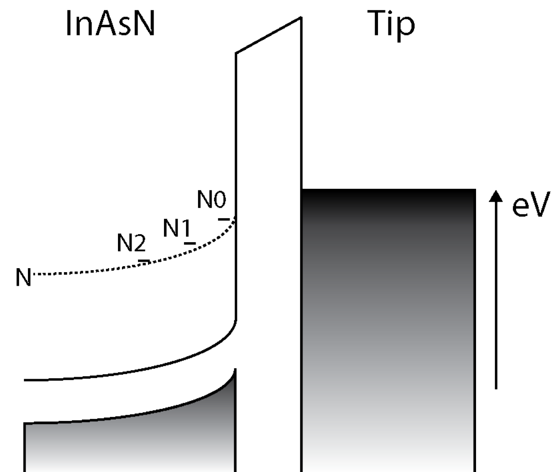

FIG. 5. Schematic band diagram of a STM tip in contact with N-doped InAs. The state introduced by N is indicated by the dotted line. Tip induced band bending at positive bias pulls the bands of the sample up. Causing an energetic shift of the N atoms, depending on their distance to the surface. Energies are not to scale.

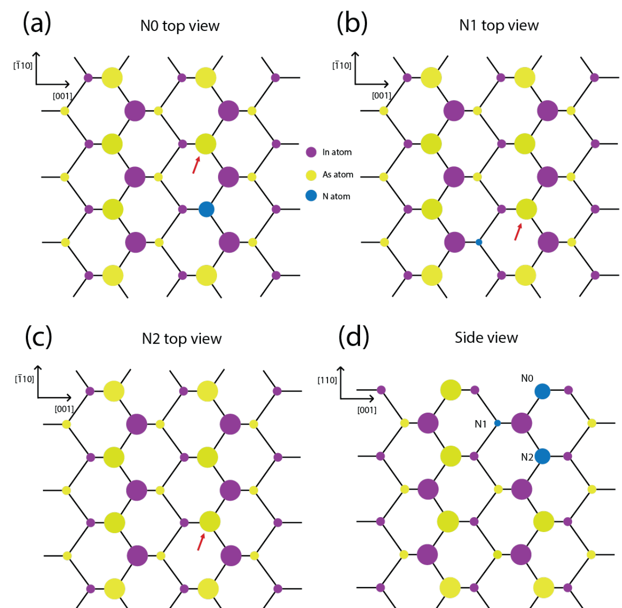

FIG. 6. In (a), (b) and (c), a schematic view of the (110) surface of the three different doped supercells is presented. The red arrows indicate which atomic position is used to calculate the LDOS for that specific cell. In (d), a side view of a (110) surface is presented to indicate at what positions the N dopants are present for the different doped supercells. The smaller Ga and As atoms shown here are present in lower lying atomic layers compared to the larger drawn Ga and As atoms.

The supercells represented schematically in Fig. 6 are used to calculate the LDOS at the atomic positions indicated by the red arrows. These specific atomic positions are chosen since at these positions the N atoms shows the strongest signature. As can be seen in figure 2, the signature is strongest on the first nearest neighbor As atom in the [$\bar{1}$10] direction

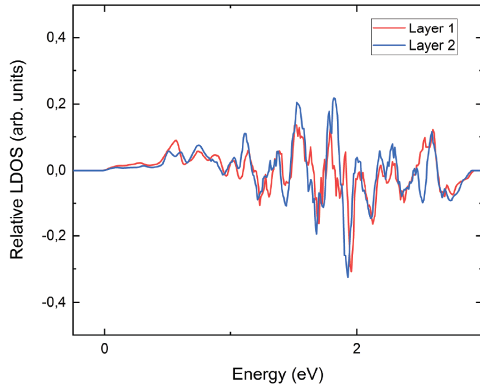

FIG. 7. LDOS calculated on the atomic positions indicated by the red arrows in Fig. 6 with the reference LDOS on the same atomic position in the reference cell subtracted from it for N1 and N2. The Fermi energy is set to 0 eV in these graphs.

in case of a surface layer N dopant. For a N dopant 1 layer below the surface, the signature is strongest on the nearest 2 As atoms that are off-center in the [001] direction while for the N2 dopant, the signature is strongest right on top of the N dopant. This is important because the STS spectra shown in Fig. 4 are measured on the areas of brightest contrast in the STM measurements. For each of these atomic positions, the LDOS is now calculated as a function of energy. From these LDOS curves we subtract the LDOS of the As atom on the same position in the lattice in the reference cell in order to highlight the changes in LDOS due to the N dopant.

In Fig. 7 the results of these calculations are shown for a N dopant 1 layer below the surface layer, N1, and 2 layers below the surface layer, N2. The results including the surface layer N dopant, N0, are shown in the supplemental material for completeness[36]. The results regarding the surface layer N dopant are not explicitly discussed here since a surface layer dopant is known to exhibit more complex behavior due to its interaction with the surface relaxation and different coordination from the N dopants deeper below the surface. This is for instance the case for the bi-stability of Si in GaAs and the Ga vacancy in m-plane GaN[3738]. The LDOS graphs shown in Fig. 7 show that the electronic signature of a N dopant 1 or 2 layers below the surface is very similar. It is not prudent to directly compare these curves to the curves shown in Fig. 4. The TIBB of the STM tip can greatly influence where exactly we see the signature of these states as well as the work function of the tip used. Also, the DFT calculations show an incorrect band gap which can influence the absolute enregetic position of different states in DFT. We do not observe a single very sharp peak in LDOS like observed for the STM measurements followed by a decrease like seen in Fig. 4. We do however see several smaller peaks in LDOS that are each followed by a decrease in LDOS, the deepest of which is present at 1.96 eV and 1.93 eV for layer 1 and layer 2 respectively. These calculations indicate that it is indeed possible for this shift of LDOS to be energetic rather than spatial and that the layer 1 and layer 2 N dopants have very similar effects on the LDOS on the surface atoms. There is in fact close to no change in the energetic position of the state between the two. Experimentally, however, we found an increasing energy with increasing dopant depth from the surface as shown in Fig. 4. This observed experimental trend therefore has to be caused by TIBB. TIBB pulls the bands of InAs and the N states contained within, up, when measuring at positive bias. This effect is strongest at the surface and decays when going deeper into the bulk, as schematically shown in Fig. 5. This is also observed for N atoms in GaAs, although not structurally with STS measurements[16,17]. For donors in the (110) surface of GaAs it has been observed that the binding energy is increased compared to lower lying donors[39,40]. We do not see evidence for an increased resonance energy of the surface N, but a minor change could be hidden underneath the effects of the TIBB.

E. CITS maps

Current imaging tunneling spectroscopy (CITS) maps are obtained by plotting a sub-grid over a normal STM image and obtaining an STS curve at each of the points of the sub-grid. This results in spatial image with I/V and dI/dV information at each point. Due to the time it takes to obtain a single STS curve, the time to obtain a CITS map quickly rises as the resolution increases. Since the single STS spectra of Fig. 4 already provide us with a direct comparison of the spectroscopic states of N atoms at different layers below the surface, we chose to make high-resolution CITS maps of single N atoms in different layers instead of making one map containing all of them. This means that energy levels between the CITS maps of different N atoms cannot directly be compared, since the tip may have changed in between. Instead we discuss the spatial and energetic features observed per atom. The CITS data is always displayed as a cut of the the full data set. Since the data set has an STS spectrum on a x and y grid, this means that the full data set has 4 dimensions x, y, V and dI/dV. A cut at a specific voltage will be displayed as a XY color plot of dI/dV values. Cuts can also be made along the spatial directions x or y, plotted as a XV or YV color plots. Lastly also single STS spectra can be extracted at specific (x, y) coordinates, which are displayed as standard (dI/dV) graphs. CITS maps of N0 and N1 can be found in the Supplemental Material[36].

1. N2

In Figure 8(a) a XY cross-section of a CITS map of an N atom two layers below the surface is displayed at a bias of $+1.8$ V. Observable in this image are the area which is defined as the InAs background, recognizable by the green rectangle and the (x, y) coordinate where a single spectrum of the N atom is extracted, as marked with the white dot. Two cuts of the CITS map as marked by the dashed white lines are marked with 'Cut' and X. The characteristic bow-tie like shape of the N atom two layers below the surface can be observed by its

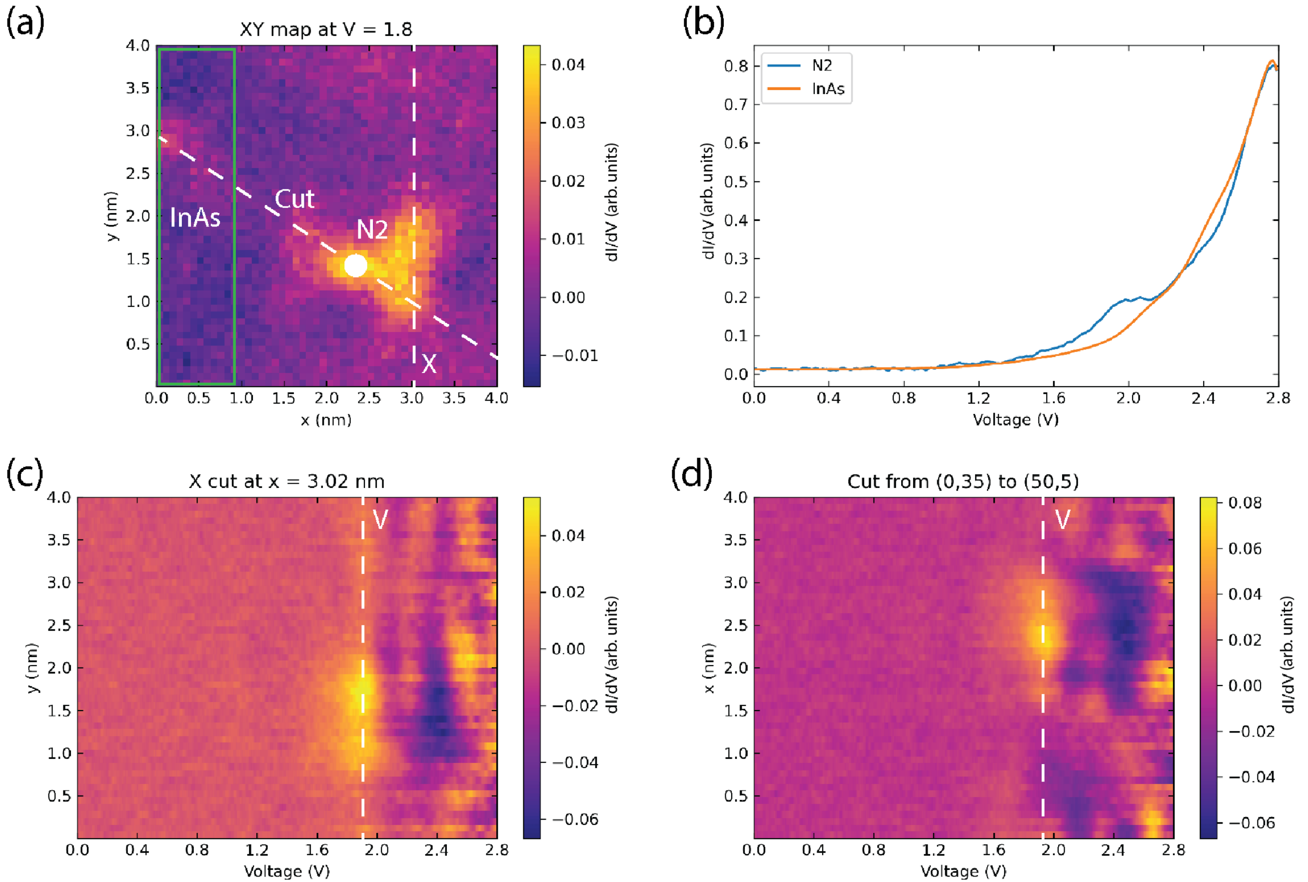

FIG. 8. CITS (dI/dV) data set of an N atom two layers below the surface, displayed as different cuts. (a) XY map at a bias of +1.8 V. (b) STS spectra obtained on the layer 2 N atom (N2) and the InAs background as averaged over the green rectangle in (a). (c) and (d) Cuts of (a) along the dashed white line marked with X and Cut, respectively. The voltage at which the cut of (a) is obtained is indicated by the white dashed line marked with V. The InAs background has been subtracted to highlight changes induced by the N atom.

bright contrast. Figure 8(b) displays the STS spectrum taken on the center of the N atom and the average of the STS spectra in the green rectangle in Fig. 8(a) in blue and orange, respectively. Here it can be observed that from +1.4 to +2.1 V the dI/dV signal on the N atom is stronger than on the InAs, while between +2.3 and +2.6 V it is weaker. At the stabilizing voltage of +2.8 the dI/dV signals of the of N atom and the background have the same strength, indicating minimal crosstalk. The peak of the enhancement lies at +1.8 V, which is different from the +1.5 V observed in Fig. 4, indicating again that the tip state has a strong influence on the resonant states.

The cut displayed in Fig. 8(c) is made along the dashed white line in Fig. 8(a) marked with X. Here the two rightmost lobes of the bowtie can be observed at x equals 1 and 1.8 nm and a bias of +1.8 V. Around +2.4 V a decrease of the dI/dV signal is observed at the same location.

In Fig. 8(d) a cut of 8(a) is displayed along the dashed white line marked with Cut. The plot in Fig. 8(d) is obtained by taking a spectrum at each x coordinate that lies closed to the dashed line, in this way the total length in x is still 4 nm. Around x equals 1.8 the first weak lobe of dI/dV contrast can be observed at a bias of +1.8 V. The strongest contrast is observed at x equals 2.3 and the third, weaker, lobe around 2.8.

At the location of this enhanced contrast, a drastically different effect can be observed at higher voltages. Around +2.5 V the dI/dV signal is reduced compared to the InAs background. This can be seen in Fig. 8(b), 8(c) and 8(d). In Fig. 9 the spatial cut of the CITS map at +2.5 is displayed. Here it can clearly be observed that the reduction of the dI/dV signal has the same shape and spatial extend as the enhancement observed in Fig. 8(a).

2. *Discussion*

The characteristic shapes of the N impurities as observed in Fig. 2 can clearly be recognized in the CITS maps as an enhancement of the dI/dV signal. For all CITS maps we see a reduction of the dI/dV signal at voltages above the resonance. The reduction shifts to lower energies with increasing depth of the N atoms, just as the resonance energy. The spatial extension of the reduction is the same as the characteristic enhancement, as can be seen when comparing Fig. 8(a) and Fig. 9. This corresponds nicely with the prediction made by the DFT

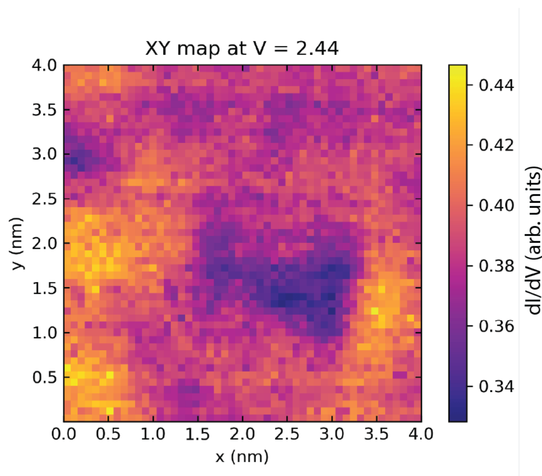

FIG. 9. CITS cut at +2.44 V of the same data set as Fig. 8, containing an N atom two layers below the surface. The reduction of the dI/dV signal below the InAs background can be observed as the dark colored area.

calculations in section III C. For this N impurity, topography cross-talk can be eliminated as a cause of this reduction since at the stabilizing voltage of +2.8 V the dI/dV signal on the impurity and on the InAs background are equal. We explain this reduction by considering the influence of an individual N impurity on the LDOS of the InAs host. For individual N impurities the effect is described by a redistribution of states, moving host states with a higher energy than the N level to the N level[41]. The fact that the reduction has the same shape and spatial extend as the characteristic enhancement shows that this redistribution is energetic in nature.

IV. CONCLUSIONS

We studied iso-electronic N impurities in InAs at the atomic scale to see how iso-electronic impurities behave deep in the conduction band. STS curves obtained on undoped InAs and N-doped InAs show a small band gap reduction of <0.1eV. The full effect of the expected 20% band gap reduction is not observed here due to limited current resolution for very low positive bias and tip-sample interaction. The signatures of the N atoms at both filled and empty state imaging are remarkably similar to N atoms in GaAs. The signatures at empty state imaging were also compared to DFT simulations and showed an excellent correspondence. The main difference is that in InAs the N state is located deeper into the conduction band, making it possible to image conduction band states below the N level. STS measurements performed on N atoms up to two layers below the (110) surface of InAs show a reduction of the resonance energy of the N atom with increasing depth. This is attributed to TIBB, pulling the N states up at positive bias and acting most strongly on surface N atoms. This behavior is also supported by the DFT calculations showing similar surface LDOS behavior for N dopants at different depths below the surface. CITS maps of N atoms up to two layers below the surface give a high resolution spatial and spectroscopic overview of the N atoms. Here the characteristic shape of the N atoms in different layers below the surface is observed as an enhancement of the dI/dV signal compared to the InAs background. At energies above the enhancement a reduction of the dI/dV is observed, which has the same shape and size as the enhancement. This shows that the redistribution of states caused by the N impurities is mostly energetic in nature.

ACKNOWLEDGMENTS

We would like to acknowledge Zhanguo Li and Zhongmei Huang for their assistance with the growth of the material at Lancaster University. We thank the Nederlandse Organisatie voor Wetenschappelijk onderzoek (NWO) for funding this research through Zwaartekracht project on Integrated Nanophotonics with Project No. [10018478] and for also providing the computational resources needed for this study. NWO granted us access to the Snellius supercomputer in Amsterdam through project EINF-3528 which was used to carry out the DFT calculations. To the support from Province-City Cooperation Project of Construction of Guangxi Key Laboratory of Machine Vision And Intelligent ControlGrant Nos.GKAD20297148. Author T.J.F. Verstijnen and D. Tjeertes have contributed equally to the work presented here.

* t.j.f.verstijnen@tue.nl

[1] M. Weyers, M. Sato, and H. Ando, Japanese Journal of Applied Physics **31**, L853 (1992), iSBN: 0021-4922.

[2] W. Shan, W. Walukiewicz, J. W. Ager, E. E. Haller, J. F. Geisz, D. J. Friedman, J. M. Olson, and S. R. Kurtz, Physical Review Letters **82**, 1221 (1999), iSBN: 1521-3951.

[3] W. Shan, W. Walukiewicz, J. W. Ager, E. E. Haller, J. F. Geisz, D. J. Friedman, J. M. Olson, and S. R. Kurtz, Journal of Applied Physics **86**, 2349 (1999), iSBN: 0021-8979.

[4] J. Wu, W. Shan, and W. Walukiewicz, Semiconductor Science and Technology **17**, 860 (2002).

[5] A. Lindsay and E. P. O'Reilly, Physical Review Letters **93**, 196402 (2004), publisher: American Physical Society.

[6] A. Lindsay and E. P. O'Reilly, Physica E: Low-dimensional Systems and Nanostructures Proceedings of the Eleventh International Conference on Modulated Semiconductor Structures, **21**, 901 (2004).

[7] Y. Zhang, B. Fluegel, A. Mascarenhas, H. P. Xin, and C. W. Tu, Phys. Rev. B **62**, 4493 (2000).

[8] X. Liu, M. Pistol, L. Samuelson, S. Schwetlick, and W. Seifert, Applied Physics Letters **56**, 1451 (1990).

[9] J. D. Perkins, A. Mascarenhas, Y. Zhang, J. F. Geisz, D. J. Friedman, J. M. Olson, and S. R. Kurtz, Physical Review Letters **82**,

3312 (1999).
[10] D. K. Shih, H. H. Lin, L. W. Sung, T. Y. Chu, and T. R. Yang, Japanese Journal of Applied Physics, Part 1: Regular Papers and Short Notes and Review Papers **42**, 375 (2003).
[11] E. P. O'Reilly, A. Lindsay, P. J. Klar, A. Polimeni, and M. Capizzi, Semiconductor Science and Technology **24** (2009), 10.1088/0268-1242/24/3/033001.
[12] H. A. McKay, R. M. Feenstra, T. Schmidtling, and U. W. Pohl, Applied Physics Letters **78**, 82 (2001).
[13] H. A. McKay, R. M. Feenstra, T. Schmidtling, U. W. Pohl, and J. F. Geisz, Journal of Vacuum Science & Technology B: Microelectronics and Nanometer Structures **19**, 1644 (2001).
[14] J. M. Ulloa, P. M. Koenraad, and M. Hopkinson, Applied Physics Letters **93**, 1 (2008).
[15] F. J. Tilley, M. Roy, P. A. Maksym, P. M. Koenraad, C. M. Krammel, and J. M. Ulloa, Phys. Rev. B **93**, 035313 (2016).
[16] N. Ishida, M. Jo, T. Mano, Y. Sakuma, T. Noda, and D. Fujita, Nanoscale **7**, 16773 (2015), publisher: Royal Society of Chemistry.
[17] R. C. Plantenga, V. R. Kortan, T. Kaizu, Y. Harada, T. Kita, M. E. Flatté, and P. M. Koenraad, Phys. Rev. B **96**, 155210 (2017).
[18] J. Ibáñez, R. Oliva, M. De la Mare, M. Schmidbauer, S. Hernández, P. Pellegrino, D. J. Scurr, R. Cuscó, L. Artús, M. Shafi, R. H. Mari, M. Henini, Q. Zhuang, A. Godenir, and A. Krier, Journal of Applied Physics **108**, 103504 (2010).
[19] F. Filippone, G. Mattioli, A. Polimeni, M. Felici, and A. A. Bonapasta, The Journal of Physical Chemistry C **124**, 19240 (2020).
[20] G. Kresse and J. Furthmüller, Phys. Rev. B **54**, 11169 (1996).
[21] J. P. Perdew, K. Burke, and M. Ernzerhof, Phys. Rev. Lett. **77**, 3865 (1996).
[22] P. E. Blöchl, Phys. Rev. B **50**, 17953 (1994).
[23] J. G. Lee, *Computational materials science: an introduction* (CRC press, 2016).
[24] J. D. Pack and H. J. Monkhorst, Phys. Rev. B **16**, 1748 (1977).
[25] N. N. Anua, R. Ahmed, A. Shaari, M. A. Saeed, B. U. Haq, and S. Goumri-Said, Semiconductor Science and Technology **28**, 105015 (2013).
[26] R. M. Feenstra, S. Gaan, G. Meyer, and K. H. Rieder, Phys. Rev. B **71**, 125316 (2005).
[27] R. M. Feenstra, Y. Dong, M. P. Semtsiv, and W. T. Masselink, Nanotechnology **18**, 044015 (2006).
[28] N. Ishida, K. Sueoka, and R. M. Feenstra, Phys. Rev. B **80**, 075320 (2009).
[29] C. A. Mead and W. G. Spitzer, Physical Review Letters **10**, 471 (1963), publisher: American Physical Society.
[30] S. Kawaji and H. C. Gatos, Surface Science **7**, 215 (1967).
[31] L. O. Olsson, C. B. M. Andersson, M. C. Håkansson, J. Kanski, L. Ilver, and U. O. Karlsson, Phys. Rev. Lett. **76**, 3626 (1996).
[32] J. R. Weber, A. Janotti, and C. G. Van de Walle, Applied Physics Letters **97** (2010), 10.1063/1.3518061, 192106, https://pubs.aip.org/aip/apl/article-pdf/doi/10.1063/1.3518061/14439068/192106_1_online.pdf.
[33] R. Dombrowski, C. Steinebach, C. Wittneven, M. Morgenstern, and R. Wiesendanger, Physical Review B **59**, 8043 (1999), publisher: American Physical Society.
[34] J. Ibáñez, R. Oliva, M. De la Mare, M. Schmidbauer, S. Hernández, P. Pellegrino, D. J. Scurr, R. Cuscó, L. Artús, M. Shafi, R. H. Mari, M. Henini, Q. Zhuang, A. Godenir, and A. Krier, Journal of Applied Physics **108** (2010), 10.1063/1.3509149, 103504, https://pubs.aip.org/aip/jap/article-pdf/doi/10.1063/1.3509149/14810601/103504_1_online.pdf.
[35] L. Ivanova, H. Eisele, M. P. Vaughan, P. Ebert, A. Lenz, R. Timm, O. Schumann, L. Geelhaar, M. Dähne, S. Fahy, H. Riechert, and E. P. O'Reilly, Phys. Rev. B **82**, 161201(R) (2010).
[36] See Supplemental Material at [URL will be inserted by publisher] for additional supporting figures.
[37] A. P. Wijnheijmer, J. K. Garleff, K. Teichmann, M. Wenderoth, S. Loth, and P. M. Koenraad, Phys. Rev. B **84**, 125310 (2011).
[38] J.-M. Hyun and H. Kim, Journal of the Korean Physical Society **68**, 420 (2016).
[39] A. P. Wijnheijmer, J. K. Garleff, K. Teichmann, M. Wenderoth, S. Loth, R. G. Ulbrich, P. A. Maksym, M. Roy, and P. M. Koenraad, Phys. Rev. Lett. **102**, 166101 (2009).
[40] D. Tjeertes, A. Vela, T. J. F. Verstijnen, E. G. Banfi, P. J. van Veldhoven, M. G. Menezes, R. B. Capaz, B. Koiller, and P. M. Koenraad, Physical Review B **104**, 125433 (2021), publisher: American Physical Society.
[41] P. R. C. Kent and A. Zunger, Phys. Rev. B **64**, 115208 (2001).